separations

MDPI

Article

Applicability Evaluation of Demulsification Processes and Optimization of Centrifugal Demulsification Parameters for Highly Emulsified Crude Oil from the Shixi Operation Area

Lujun Liu [1], Bodong Li [1], Xin Peng [1], Xianglu Yang [2], Yanxin Li [1], Jiaxin Wei [1] and Junwei Hou [1,*]

[1] State Key Laboratory of Heavy Oil Processing, China University of Petroleum (Beijing) at Karamay, Karamay 834000, China
[2] Shunan Gas Mine, PetroChina Southwest Oil and Gasfield Company, Luzhou 646000, China
* Correspondence: junweihou@cupk.edu.cn

Abstract

To address the difficulty of demulsifying a water-in-oil (W/O) crude oil emulsion with a high solids content from the Shixi Operating Area, the adaptability of electrostatic dehydration, ultrasonic demulsification, and centrifugal demulsification was compared. A centrifugal demulsification process combined with additives was optimized using response surface methodology and single-factor experiments. The results showed that the emulsion contained substantial amounts of resins, asphaltenes, and inorganic solids, including FeS and carbonates. The small density difference between oil and water further impeded their separation. The maximum demulsification efficiencies of conventional electrostatic dehydration and ultrasonic treatment were only 52.6% and 40%, respectively, and could not meet the treatment requirements. Optimal process conditions were obtained using a Box–Behnken response surface design. Under moderately effective baseline conditions, appropriate dosages of 2.0% sodium silicate and 40 mg·L^{-1} SP169 were identified. When the optimized process and additives were combined for validation, the mean demulsification efficiency calculated from the volume of separated free water reached 93.5 ± 0.30%. Microscopic observations indicated that the centrifugal force field could disrupt the solid–organic matter emulsified aggregate structure in the system. The optimized centrifugal demulsification process combined with additives showed good adaptability to this type of crude oil emulsion with a high solids content and may provide a reference for demulsification treatment in the field and for similar emulsions.

Keywords: highly emulsified crude oil; high-solids water-in-oil emulsion; centrifugal demulsification; response surface optimization; additives; oil–water separation

Check for updates

Academic Editor: Victoria Samanidou

Received: 30 September 2026
Revised: 22 October 2026
Accepted: 27 October 2026
Published: 29 October 2026

Copyright: © 2026 by the authors. Licensee MDPI, Basel, Switzerland. This article is an open access article distributed under the terms and conditions of the Creative Commons Attribution (CC BY) license.

1. Introduction

During crude oil production, gathering, transportation, and treatment, crude oil can mix thoroughly with aqueous phases such as formation water, fracturing flowback fluid, workover fluid, and chemical flooding fluid. Shear generated by pipeline transportation, pumping, and equipment disturbance then forms stable oil–water emulsions [1–4]. In water-in-oil emulsions, fine water droplets are dispersed in a continuous oil phase. This not only increases the water content, apparent viscosity, and transportation energy consumption of crude oil but can also cause equipment corrosion, scaling, a decline in the treatment capacity of settling equipment, and an excessive water content in crude oil delivered for export. Efficient oil–water separation and suspended-solid removal are therefore important

for maintaining stable operation of oilfield surface gathering and transportation systems, reducing treatment costs, and meeting quality requirements for exported crude oil.

The stability of crude oil emulsions is jointly affected by numerous factors, including crude oil composition, dispersed water droplet size, the oil–water density difference, interfacial tension, interfacial electrical properties, and solid particle content [5,6]. Natural surface-active components in crude oil, such as asphaltenes, resins, waxes, and naphthenic acids, can adsorb at the oil–water interface and form an interfacial film with a certain strength and viscoelasticity, hindering contact and coalescence between water droplets [7–11]. Previous studies generally consider asphaltenes to be important components stabilizing oil-in-water emulsions, while resins can affect the interfacial aggregation behavior and film structure of asphaltenes through dissolution, dispersion, or cooperative adsorption. At the same time, fine solids such as clay, silica, corrosion products, inorganic salts, and scale particles may participate in oil–water interfacial interactions and act together with asphaltenes and resins to increase emulsion stability [12–15]. Thus, the stability of crude oil emulsions with high solids contents is likely to result from the combined effects of natural organic surface-active components and inorganic solid particles.

Current methods for demulsifying crude oil emulsions mainly include chemical demulsification, thermochemical demulsification, electrostatic dehydration, ultrasonic demulsification, and centrifugal separation. Chemical demulsifiers can weaken the interfacial film through interfacial adsorption, diffusion, and displacement and promote droplet coalescence, but their treatment effectiveness is readily affected by crude oil composition, emulsion aging, demulsifier structure, and dosage [16–18]. When an emulsion contains many solid particles, the ability of conventional demulsifiers to disrupt the particle–organic matter composite interfacial film may be limited [19–21]. Electrostatic dehydration mainly uses an electric field to promote water droplet polarization and coalescence [22], but conductive particles such as FeS may cause a nonuniform electric field and reduce operational stability. Ultrasonic demulsification promotes droplet coalescence through cavitation, mechanical vibration, and interfacial disturbance. Its effectiveness is affected by frequency, power, temperature, and treatment time [23], and its adaptability to high-strength composite interfacial films remains limited. In comparison, centrifugal separation can substantially increase the driving force for migration and settling of the oil and water phases and solid particles, with the potential to shorten separation time and intensify dehydration and solid removal. It is therefore suitable for treating highly stable crude oil emulsions with high solids contents [24].

At present, systematic research remains lacking on the stable structures and intensified demulsification mechanisms of highly emulsified systems in low-viscosity crude oil that are jointly stabilized by inorganic solid particles, asphaltenes, and resins. In particular, when the oil–water density difference is small, dispersed water droplets are fine, and the suspended matter content is high, gravitational settling is weakened and the composite interfacial film further inhibits droplet coalescence, making it difficult for conventional thermochemical demulsification to achieve satisfactory results. It is therefore necessary to combine analyses of crude oil properties, interfacial characteristics, and microscopic morphology to identify the principal stabilizing factors and select an appropriate intensified separation process.

In recent years, emulsion systems stabilized in part by inorganic solid particles have attracted increasing attention in petroleum production. Sun et al. [12] found that silica nanoparticles and asphaltenes could co-adsorb at the oil–water interface and form a rigid composite film, substantially increasing the stability of emulsions in a heavy crude oil system and reducing demulsification efficiency by more than 40%. Hattori et al. [13] studied crude oil emulsions with suspended solids contents above 500 mg/L and found that the

interfacial viscoelastic modulus increased by a factor of 2–3, while conventional chemical demulsifiers achieved a demulsification efficiency of less than 30%. Centrifugal separation has shown a distinct advantage for high-solids emulsions: Wang et al. [24] developed a miniaturized centrifugal demulsification device that achieved more than 85% oil–water separation efficiency within 10 min for a highly stable crude oil emulsion affected by solid particles, a result 2–3 times that of gravitational settling. These studies provide important references for treating high-solids emulsions, but most have addressed systems with relatively large oil–water density differences. By contrast, the Shixi crude oil emulsion investigated here has a smaller oil–water density difference and a higher suspended-solids content. Under the experimental conditions of this study, centrifugation coupled with combined additives achieved a demulsification efficiency above 93%, exceeding the treatment effects of conventional chemical demulsification and centrifugal separation alone reported in the studies cited above. The mechanism of action is shown in Figure 1. Therefore, studying the demulsification of emulsions with small density differences and high solids contents from the Shixi area has engineering value.

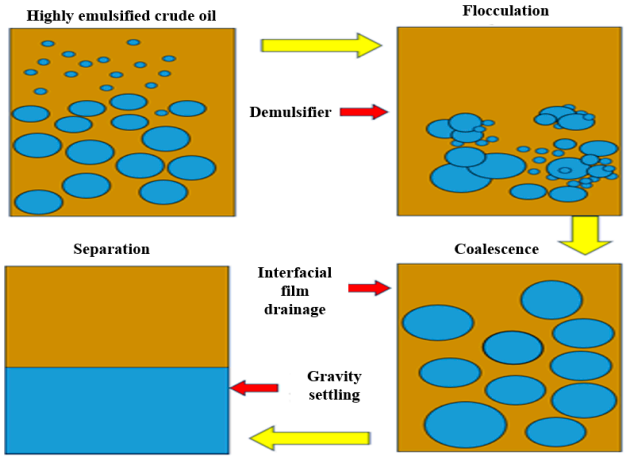

Figure 1. Demulsification and dehydration process for highly emulsified crude oil.

Based on the emulsion stabilization and demulsification mechanisms described above, this study used highly emulsified crude oil from the Shixi Operating Area as the research subject. Its basic physical properties, interfacial characteristics, suspended-solid composition, and microscopic morphology were analyzed to explore the causes of its high stability. Three demulsification processes—electrostatic dehydration, ultrasonication, and centrifugation—were compared. Single-factor experiments and response surface methodology were used to examine the effects of centrifugal speed, system temperature, and demulsifier concentration on demulsification, followed by optimization of process parameters including sodium silicate, SP169, and centrifugation time. The results showed that solid particles markedly enhanced the emulsification of this crude oil and that intensified centrifugal demulsification produced better oil–water separation than electrostatic dehydration and ultrasonic treatment. This study provides a reference for selecting demulsification processes and optimizing laboratory process parameters for highly emulsified crude oil with a high solids content from light-oil blocks.

2. Materials and Methods

2.1. Experimental Materials and Instruments

The highly emulsified crude oil used in the experiments was a water-in-oil (W/O) emulsion collected from the emulsified layer of a settling tank at the centralized treatment station in the Shixi Operating Area of the Xinjiang Oilfield. After collection, samples

were immediately sealed, refrigerated at 4 °C, and used for all experiments within 7 days. Before the experiments, samples were aged in a constant-temperature water bath (SB-2100, Shanghai Anting Scientific Instrument Factory, Shanghai, China) at 45 °C for 24 h. Before each experiment, they were manually inverted 100 times to ensure homogeneity. Industrial-grade demulsifier I was supplied by the Shixi Operating Area of the Xinjiang Oilfield (Karamay, China); industrial-grade sodium silicate was purchased from Wuxi Quecheng Silica Chemical Co., Ltd. (Wuxi, China); industrial-grade cationic flocculant SP169 was purchased from Gongyi Xinqi Chemical Plant (Gongyi, China); analytical-grade anhydrous ethanol was purchased from Sinopharm Chemical Reagent Co., Ltd. (Shanghai, China); industrial-grade unleaded gasoline was obtained from Xinjiang Oilfield Company (Karamay, China); and deionized water used in the experiments was prepared on-site with an UPR-II-10TNP pure-water unit (Chengdu Ultrapure Technology Co., Ltd., Chengdu, China).

A rheometer (MCR 102, Anton Paar Shanghai Trading Co., Ltd., Shanghai, China) was used to measure the rheological properties of the crude oil; an automatic surface tensiometer (QBZY-1, Shanghai Fangrui Instrument Co., Ltd., Shanghai, China) was used to measure the oil–water interfacial tension between the highly emulsified crude oil emulsion and the aqueous phase; and an optical microscope (AxioScope series, Carl Zeiss, Oberkochen, Germany) was used to observe emulsion microstructure. Electrostatic dehydration experiments were conducted with a high-frequency pulsed electrostatic dehydration tester (JFY-6BH, Taizhou Jiangyan Analytical Instrument Factory, Taizhou, China). Ultrasonic demulsification experiments were conducted with a bath-type ultrasonic reactor rather than a probe-type reactor (UH500AIO, rated power 500 W, Shanghai Ouhor Machinery Equipment Co., Ltd., Shanghai, China). Centrifugal demulsification experiments used a high-speed benchtop centrifuge (Centrifuge 5810 R, equipped with an F-34-6-38 fixed-angle rotor, rated maximum speed 12,000 r/min, Eppendorf SE, Hamburg, Germany). A crude oil water-content analyzer (JSH3202, Jinshi Petrochemical Instrument Co., Ltd., Jinshi, China) measured crude oil water content; a constant-temperature water bath (SB-2100, Shanghai Anting Scientific Instrument Factory, Shanghai, China) controlled system temperature; and a multipurpose shaker (20 mm amplitude, Jintan Huacheng Runhua Experimental Instrument Factory, Jintan, China) mixed samples and reagents.

2.2. Experimental Methods

To compare the applicability of different physically intensified processes to highly emulsified Shixi crude oil, electric-field demulsification, ultrasonic demulsification, and centrifugal demulsification experiments were conducted separately. Unless otherwise stated, all experiments used highly emulsified crude oil samples from the same batch, and the samples were thoroughly mixed before each experiment. Demulsifier and additives were added at the specified concentrations and mixed uniformly by shaking. Each demulsification experiment included three parallel replicates, and the experimental result was the mean of the three measurements.

Because the field heating temperature usually does not exceed 80 °C, an experimental temperature range of 45–80 °C was used to investigate the effect of temperature under heated conditions. The results showed that the apparent viscosity of the emulsion exceeded 34 mPa·s at room temperature (25 °C) and fell below 11 mPa·s at temperatures of 45 °C or above. Considering the high viscosity, high mass-transfer resistance, and poor demulsification performance of the emulsion at room temperature, 45 °C was selected as the lower starting temperature of the experiments.

2.2.1. Electrostatic Dehydration Demulsification Experiments

Electrostatic dehydration experiments were conducted with a laboratory high-frequency pulsed electrostatic dehydration tester. The device used parallel-plate stainless-steel electrodes, each measuring 80 mm × 60 mm, with an electrode spacing of 20 mm. Its output was a high-frequency pulsed voltage at 2 kHz. The voltages applied across the electrodes were set at 1.00 and 5.85 kV. Calculated using E = U/d, the two voltages corresponded to nominal average electric field strengths of 0.500 and 2.925 kV·cm^{-1}, respectively, where d was 2.0 cm. These field strengths were nominal values calculated from the electrode spacing; the actual local electric field may have been affected by electrode edge effects, emulsion heterogeneity, and the distribution of solid particles.

For each experiment, the emulsion containing the specified demulsifier concentration was thoroughly shaken, transferred to the electrostatic dehydration reaction vessel, and sealed. After the heating system brought it to the target temperature, the high-voltage pulsed power supply was switched on and gradually adjusted to the target voltage. A voltage of 5.85 kV was the highest applied voltage examined in this study and the highest voltage setting the device could reach under these sample conditions. The voltage was not increased further because doing so could have triggered device protection. The volume of separated water, device output status, and protective tripping events were recorded during each experiment. A sudden decrease in output voltage or a decrease to zero, protective tripping, or an observable discharge was defined as an electric-field instability or transient breakdown event.

The experiments examined the effects of voltage (1 and 5.85 kV), system temperature (45 and 60 °C), demulsifier concentration (50–200 mg·L^{-1}), and reaction time (20, 40, and 60 min) on demulsification.

2.2.2. Ultrasonic Demulsification Experiments

A bath-type, non-probe ultrasonic reactor was used for the ultrasonic demulsification experiments. The device's automatic frequency-tracking range was 19–26 kHz, and the experimental frequency was set to 25 kHz. For each experiment, exactly 15 mL of emulsion was placed in a 50 mL graduated, sealed glass reaction tube, which was fixed in the ultrasonic bath. The position and immersion depth of the reaction tube and its relative position to the ultrasonic transducer were kept constant across all experimental groups. The instrument's set output power was 150 W. In a bath-type ultrasonic device, much of the acoustic energy is dissipated in the water-bath medium. Because of the device structure, reaction-tube position, immersion depth, and other factors, the actual acoustic power density inside the reaction tube could not be determined precisely without calorimetric calibration. This study therefore recorded the instrument panel's set power, the sample volume, and all sample placement conditions to support reproducibility. The ultrasonic bath was temperature-controlled throughout, while a thermometer monitored the temperature inside the reaction tube. During ultrasonic treatment, the difference between the measured sample temperature and the set temperature was kept within ±2 °C.

Before the formal experiments, preliminary screening assessed the effects of ultrasonic power (80–500 W) and treatment time (5–30 min). The preliminary results showed that, for this high-solids crude oil emulsion, changing only ultrasonic power or treatment time produced a very limited increase in demulsification efficiency and could not overcome the system's intrinsic separation limitation. Based on this preliminary finding, ultrasonic power and treatment time were not included as variables in the formal experiments, and the preliminary raw data are not presented in the main text. Only one representative set of operating conditions was selected, and ultrasonication was used as a reference process for a horizontal performance comparison with electrostatic dehydration and centrifugation.

For each experiment, the specified concentration of demulsifier was added to the emulsion and thoroughly mixed. The sample was transferred to the reaction tube and placed in the constant-temperature ultrasonic bath. Ultrasonic power was set to 150 W and treatment time to 10 min before treatment was started. After treatment, the volume of separated free water was read, and the residual water content of the treated oil phase was measured. Because ultrasonic shear could induce secondary emulsification, ultrasonic treatment time was limited to 10 min and used together with a demulsifier and heating.

The experiments examined the effects of system temperature (45, 60, and 80 °C) and demulsifier concentration (50–200 mg·L^{-1}) on demulsification.

2.2.3. Centrifugal Demulsification Experiments

A high-speed benchtop centrifuge was used to replace gravity with the strong centrifugal force field generated by high-speed rotation, intensifying the settling and separation of the oil and water phases and solid particles. For each experiment, exactly 15 mL of homogenized emulsion was placed in a 25 mL graduated centrifuge tube, and the specified amounts of demulsifier and additives were added. After thorough shaking, the tube was preheated in a water bath to the target temperature. The centrifuge tubes were placed symmetrically in the rotor, and the instrument was started after the speed and centrifugation time were set. Immediately after centrifugation, the tubes were removed, the volume of separated water was read, and the demulsification efficiency was calculated.

The relative centrifugal force (RCF) was calculated as follows:

$$\mathrm{RCF} = 1.118 \times 10^{-5} \times r \times n^2 \quad (1)$$

where $r = 11.5$ cm is the maximum rotor radius (from the axis of rotation to the bottom of the matching centrifuge tube), and n is the rotational speed (r/min).

The experiments examined the effects of centrifugal speed (1000–8000 r/min; RCF: 128.57–8228.48 g), system temperature (45, 60, and 80 °C), demulsifier concentration, sodium silicate additive dosage, flocculant SP169 dosage, and centrifugation time on demulsification.

2.2.4. Evaluation of Demulsification Performance

This study characterized demulsification efficiency in two ways: the volumetric method, calculated by reading the volume of separated free water; and an instrumental method, using a JSH3202 crude oil water-content analyzer to determine the residual water content of the oil phase after treatment. Thermochemical demulsification was conducted with reference to SY/T 5281-2000 [25].

The demulsification efficiency calculated by the volumetric method was as follows:

$$\eta_v = \frac{V_W}{V_O} \times 100\% \quad (2)$$

where η_v is the demulsification efficiency based on the volume of separated free water, %; V_W is the volume of separated free water, mL; and V_O is the theoretical total water volume in the emulsion system, mL. (The volumetric method counts only free water that has separated into a distinct phase. In this high-solids emulsion, some water can be trapped in solid–organic matter agglomerated oily sludge and cannot separate as free water; the volumetric method alone therefore risks overestimating demulsification efficiency. To address this limitation, the residual water content of the treated oil-phase sample was also measured using the JSH3202 water-content analyzer to cross-check the separation result).

The demulsification efficiency based on residual oil-phase water content was calculated as follows:

$$\eta_M = \frac{W_O - W_r}{W_O} \times 100\% \quad (3)$$

where η_M is the demulsification efficiency based on residual water content, %; W_O is the mass of water in the original emulsion; and W_r is the mass of residual water in the treated oil phase.

The original emulsion used in this study had an initial water content of 35.56% and an initial suspended-solids content of 8300 mg·L^{-1}. To account for water retention caused by the high solids content, an oil–water–solid three-phase material balance was performed for the optimized parallel validation experiments to assess error resulting from water retained in solid oily sludge. Except for the parallel validation experiments that report demulsification efficiency by both volumetric and mass-based methods, the demulsification efficiencies in the other single-factor and process-comparison experiments are volumetric demulsification efficiencies, η_v. Oil content in water was measured with reference to SY/T 5329-2012 [26].

3. Results and Discussion

3.1. Crude Oil Physical Properties and Analysis of Demulsification Difficulties

The sample was collected from the emulsified layer of a settling tank in the Shixi Operating Area and was a water-in-oil (W/O) emulsion. Phase inversion tests at different water contents showed that emulsion viscosity first increased and then decreased as water content increased, reaching a maximum at a water content of 50% (oil–water ratio 1:1). This is typical rheological behavior of a W/O crude oil emulsion. Below 50% water content, the system was a W/O emulsion; above 50%, it underwent phase inversion to become an O/W emulsion, as shown in Figure 2. The water content of the original sample used in this study was 35.56%, below the phase inversion point, further confirming that it was a W/O emulsion.

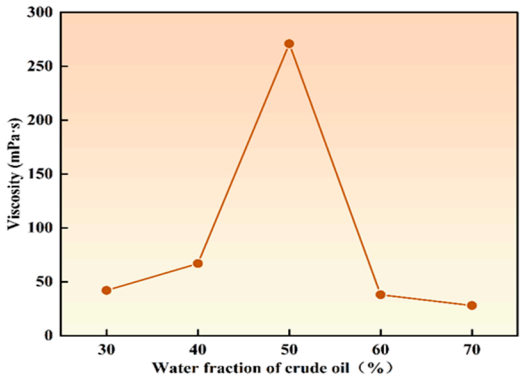

Figure 2. Phase inversion point of highly emulsified crude oil from the Shixi central processing station.

Measurements showed an emulsion density of 0.9789 g/cm^3 and an oil–water density difference of 0.0211 g/cm^3. The viscosity of the Shixi highly emulsified crude oil emulsion with a water content of 35.56% was 11 mPa·s at 40 °C. The oil–water interfacial tension was 2.4–2.7 mN/m, and the combined resin and asphaltene content of the emulsion was 9.74%. The suspended-matter content reached 8300 mg·L^{-1}. X-ray diffraction analysis showed that the suspended solids mainly comprised FeS (34%), $CaCO_3$ (24%), SiO_2 (20%), $MgCO_3$ (12%), and Al_2O_3 (10%).

Water droplet sizes in the emulsion were broadly distributed, mostly between 20 and 105 μm, and the system contained both small micrometer-scale droplets and some large droplets. Black inorganic solid particles were attached to the oil–water interface, as shown

in Figure 3. These inorganic solid particles may interact with resins and asphaltenes in the crude oil and are inferred to be an important cause of the emulsion's high stability. Although the crude oil itself was not highly viscous, the combined constraints of the broad droplet-size distribution, small oil–water density difference, high suspended-matter content, and particle–organic matter composite interfacial film made efficient oil–water separation difficult using conventional treatments. On the basis of these sample characteristics, electrostatic dehydration, ultrasonication, and centrifugation are compared below.

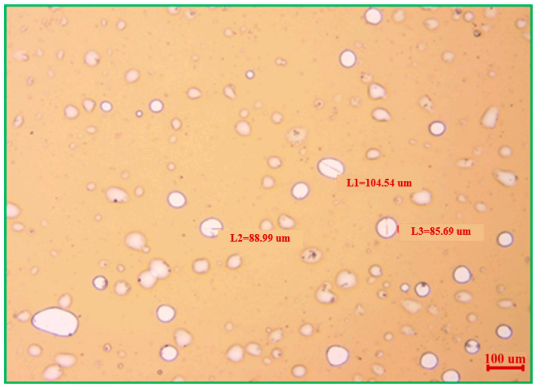

Figure 3. Microscopic morphology of highly emulsified Shixi crude oil.

3.2. Applicability Analysis of Electrostatic Dehydration Demulsification

Figure 4 shows the effects of electrostatic dehydration on highly emulsified Shixi crude oil at different voltages, temperatures, and demulsifier concentrations. Overall, demulsification efficiency gradually increased with reaction time under all experimental conditions, indicating that the electric field promoted the polarization, deformation, collision, and coalescence of dispersed water droplets in the water-in-oil emulsion [27–29]. However, the effects varied substantially among conditions because of the emulsion's stable interfacial film and conductive solid particles.

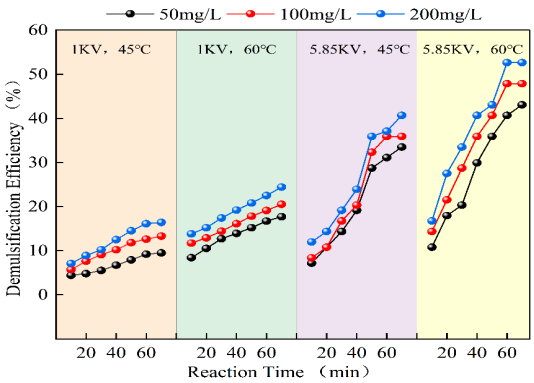

Figure 4. Variation in electrostatic dehydration demulsification efficiency with treatment time at different voltages, temperatures, and demulsifier concentrations.

At the same voltage, temperature, and reaction time, demulsification efficiency generally increased as demulsifier concentration rose from 50 to 200 mg·L^{-1}. Efficiency was highest at 200 mg·L^{-1}, followed by 100 mg·L^{-1} and then 50 mg·L^{-1}. This indicates that an appropriate increase in demulsifier concentration helps weaken the composite interfacial film formed by resins, asphaltenes, and solid particles, promoting water droplet coalescence and settling under the electric field [30,31].

Voltage substantially affected electrostatic demulsification. At 1 kV, overall demulsification efficiency was low and increased only slightly even when reaction time was extended

to 60 min. It was approximately 5–15% at 45 °C and approximately 10–25% at 60 °C. At 5.85 kV, demulsification efficiency increased much more with reaction time. The maximum efficiency was approximately 40% at 5.85 kV and 45 °C; at 5.85 kV and 60 °C, demulsification improved further and reached a maximum of 52.6%.

Increasing temperature promoted electrostatic dehydration and demulsification to some extent. At the same voltage, demulsifier concentration, and reaction time, demulsification efficiency at 60 °C was generally higher than at 45 °C. Heating can improve crude oil fluidity to some extent, promote diffusion and adsorption of demulsifier at the oil–water interface, and reduce resistance during water droplet coalescence, thereby facilitating demulsification and dehydration.

Overall, longer reaction time, higher demulsifier concentration, higher voltage, and a suitable temperature increase all improved the electrostatic demulsification efficiency of highly emulsified Shixi crude oil; voltage had the most pronounced effect. Within the experimental range, electrostatic dehydration performed best at 5.85 kV, 60 °C, 200 mg·L^{-1} demulsifier, and a reaction time of 60 min, reaching a demulsification efficiency of 52.6%. Even at the highest applied voltage achievable by this device, occasional output fluctuations and protective transient trips were observed in some parallel experiments. Together with the XRD phase-analysis results, this suggests that the large quantity of conductive FeS particles in the emulsion was an important cause of electric-field instability. Because of limitations of the experimental device, this study did not quantitatively relate FeS content, system conductivity, and the current time series; this proposed mechanism was mainly inferred from phase composition and experimental observations.

Under the optimal conditions described above, the maximum electrostatic dehydration efficiency was only 52.6%, substantially below the 93.5% achieved by the centrifugation process combined with additives. Taken together, the results obtained with this electrode configuration and device indicate limited treatment capacity under the best conditions achievable by this electrostatic dehydration process. It should be noted that electrostatic dehydration, ultrasonication, and centrifugation were each operated at their respective optimal parameters obtained from separate single-factor experiments. Strictly controlled comparisons at identical temperature, time, and reagent conditions were not conducted. The between-process comparison is therefore a horizontal reference for process screening, rather than a rigorous quantitative comparison under identical conditions. This conclusion applies only to the electrode configuration and equipment conditions used here and does not mean that other electrostatic dehydration devices or processes cannot achieve better performance.

3.3. Applicability Analysis of Acoustic Demulsification

Figure 5 shows demulsification under different demulsifier concentrations and treatment temperatures. As demulsifier concentration increased, demulsification efficiency rose at every temperature, although the magnitude of the increase differed considerably among temperatures.

At 45 °C, demulsification efficiency was generally low. As demulsifier concentration increased from 50 to 200 mg·L^{-1}, efficiency rose only from approximately 4% to approximately 7%, indicating a limited improvement from increasing concentration. At 60 °C, efficiency increased slowly with demulsifier concentration, from approximately 9% to approximately 13%, again a small overall change.

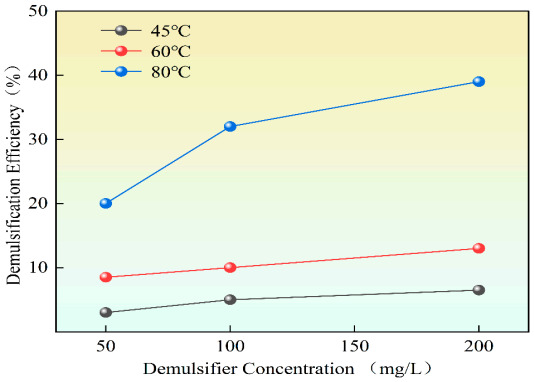

Figure 5. Variation in demulsification efficiency at different temperatures and demulsifier concentrations.

By contrast, demulsification was markedly enhanced at 80 °C. Efficiency was approximately 20% at 50 mg·L^{-1} demulsifier and rapidly increased to approximately 32% at 100 mg·L^{-1}. Further increasing concentration to 200 mg·L^{-1} raised efficiency to approximately 40%. Thus, at higher temperatures, increasing demulsifier dosage can effectively improve demulsification.

Overall, temperature had a relatively pronounced effect on demulsification. At the same demulsifier concentration, efficiencies followed the order 80 °C > 60 °C > 45 °C. The maximum, approximately 40%, occurred at 80 °C and 200 mg·L^{-1}. Therefore, within the experimental range, higher temperature and demulsifier concentration were more favorable for increasing efficiency [32–34]. In this high-solids emulsion, solid particles readily attenuated ultrasonic cavitation, and process scale-up performance was poor [33,34]. Under the ultrasonic process's own optimal conditions, the maximum demulsification efficiency was approximately 40%, which could not meet field treatment requirements. Again, this is a reference result obtained under process-screening conditions; the three processes were not operated with completely identical parameters, and their comparison serves only as a horizontal reference.

3.4. Applicability Analysis of Centrifugal Demulsification

3.4.1. Effects of Temperature, Centrifugal Speed, and Demulsifier Concentration on Demulsification Performance

To examine the effects of temperature, centrifugal speed, and demulsifier concentration on emulsion demulsification, centrifugal demulsification experiments were carried out at different values of these parameters. The results are shown in Figure 6.

Centrifugal speed had a relatively pronounced effect on demulsification. At 1000–2000 r/min (RCF: 128.57–514.28 g), efficiency was generally low, below 10%, indicating that demulsification was not apparent at low centrifugal speeds. At 3000 r/min (RCF = 1157.13 g), efficiency increased markedly, showing that increasing speed effectively promoted emulsion separation. At 4000 r/min (RCF = 2057.12 g), efficiency increased further. It was relatively high at 60 °C, approximately 60–65%, and approximately 45–62% at 45 °C and 80 °C.

At 6000 r/min (RCF = 4628.52 g), demulsification efficiencies at the different temperatures were all relatively high, approximately 80–90%, and differences among temperatures became much smaller. At 8000 r/min (RCF = 8228.48 g), efficiency remained high overall and exceeded 90% under some conditions, but the increase relative to 6000 r/min (RCF = 4628.52 g) was limited. This indicates that the benefit of further increasing centrifugal speed gradually diminished. Thus, once speed reached 6000 r/min (RCF = 4628.52 g), demulsification was essentially stable and further speed increases were of limited necessity.

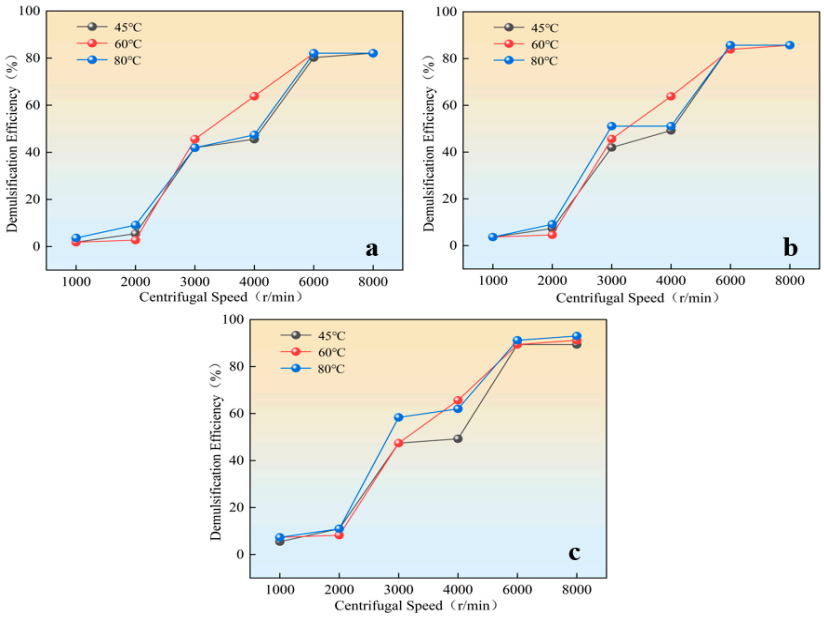

Figure 6. Effects of centrifugal speed and temperature on demulsification efficiency at different demulsifier dosages: (**a**) 50 mg·L^{-1}; (**b**) 100 mg·L^{-1}; (**c**) 200 mg·L^{-1}.

The effect of temperature on demulsification was closely related to centrifugal speed. At lower speeds, differences among temperatures were small. At 3000 r/min (RCF = 1157.13 g), efficiency was relatively high at 80 °C; at 4000 r/min (RCF = 2057.12 g), it was highest at 60 °C. At 6000–8000 r/min (RCF: 4628.52–8228.48 g), efficiencies were high at all three temperatures, and temperature-related differences narrowed further. Therefore, the effect of temperature was not simply linear but depended jointly on centrifugal speed. Within the experimental range, overall demulsification was better at 60 °C and 80 °C, although excessively high temperature did not produce a stable, sustained performance increase.

Experiments at different demulsifier concentrations showed a general increase in demulsification efficiency with concentration. The trends in the three experimental groups were essentially consistent: efficiency was low at 1000–2000 r/min (RCF: 128.57–514.28 g), rose rapidly as speed increased to 3000–4000 r/min (RCF: 1157.13–2057.12 g), and reached a high level at 6000 r/min (RCF = 4628.52 g) or above. Overall efficiencies were higher at the higher demulsifier concentration than under the other two sets of conditions and could exceed 90% at 6000–8000 r/min (RCF: 4628.52–8228.48 g), showing that increasing demulsifier concentration could improve centrifugal demulsification to some extent.

3.4.2. Process Optimization Results and Analysis Using Response Surface Methodology

On the basis of the single-factor experiments, a Box–Behnken response surface design was used to optimize the process, with centrifugal speed, system temperature, and demulsifier concentration as independent variables and demulsification efficiency as the response. The combined effects and interactions of the three factors were investigated [35,36]. Key parameters are presented in Table 1. The complete experimental matrix, significance test results, and residual diagnostic plots for the regression model are provided in Appendix A, including Tables A1 and A2, and Figure A1.

Table 1. Key statistical parameters of the response surface model.

Item	*p*-Value	Significance
Model	<0.0001	significant
Lack of fit	0.0586	not significant
$R^2 = 0.9995$		-
$R^2_{adj} = 0.9988$		-

Analysis of variance showed that the quadratic regression model was highly significant ($p < 0.0001$), while lack of fit was not significant ($p = 0.0586 > 0.05$). Both R^2 and adjusted R^2 were close to 1, indicating a good model fit and its suitability for describing how operating factors affected demulsification efficiency within the experimental range. The effects ranked as follows: A (centrifugal speed) > C (demulsifier concentration) > B (system temperature). Interaction analysis showed that the AB interaction approached significance ($p = 0.0846$), whereas AC and BC were not significant. Among the quadratic terms, A^2 and C^2 were highly significant, whereas B^2 was not significant.

The regression equation can be expressed as follows:

$$\begin{aligned} Y = &-125.20094 + 0.057277A + 0.076322B + 0.090437C \\ &+0.000015AB - 0.00000134AC + 0.0000032BC \\ &-0.000004096A^2 - 0.000718B^2 - 0.000233C^2 \end{aligned} \quad (4)$$

Note: All coefficients in this quadratic regression equation use actual physical units.

Response surfaces and contour plots are shown in Figures 7–9. Within the experimental range, demulsification efficiency increased substantially with centrifugal speed and reached a maximum near 7000 r/min (RCF = 6299.93 g). Increasing system temperature and demulsifier dosage also improved demulsification. Centrifugal speed and temperature (AB) showed a marginally significant interaction, whereas AC and BC interactions were not significant. Taken together, the preferable operating range was 6500–7500 r/min (RCF: 5432.08–7232.06 g), 70–80 °C, and a demulsifier dosage of 140–200 mg·L^{-1}, within which high demulsification efficiency could be achieved.

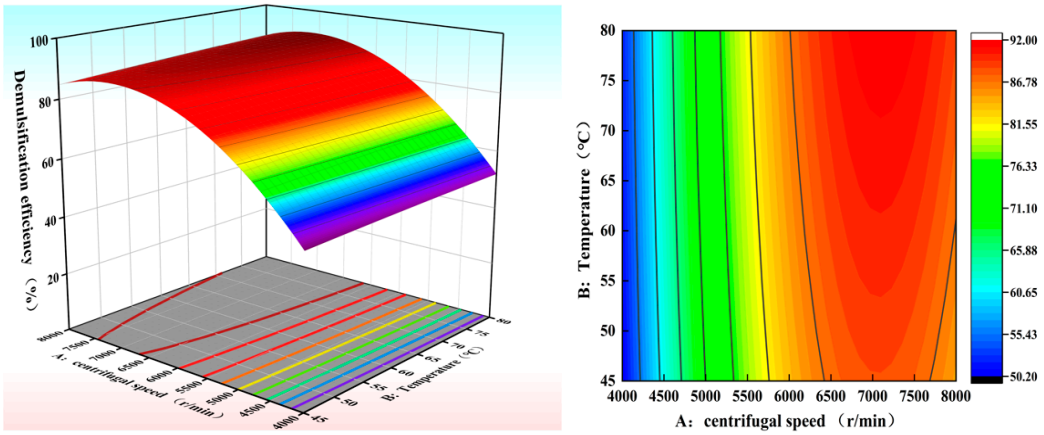

Figure 7. Three-dimensional response surface and contour plots of the RSM results: interaction effects between A and B.

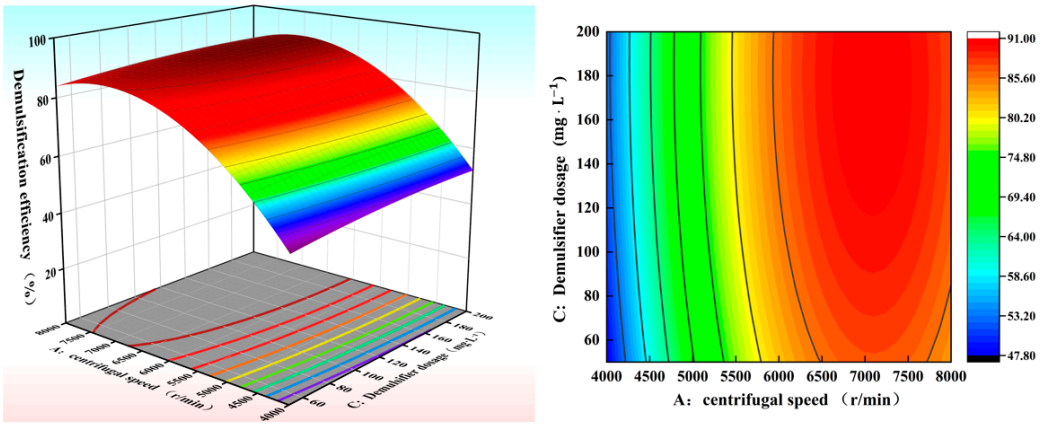

Figure 8. Three-dimensional response surface and contour plots of the RSM results: interaction effects between A and C.

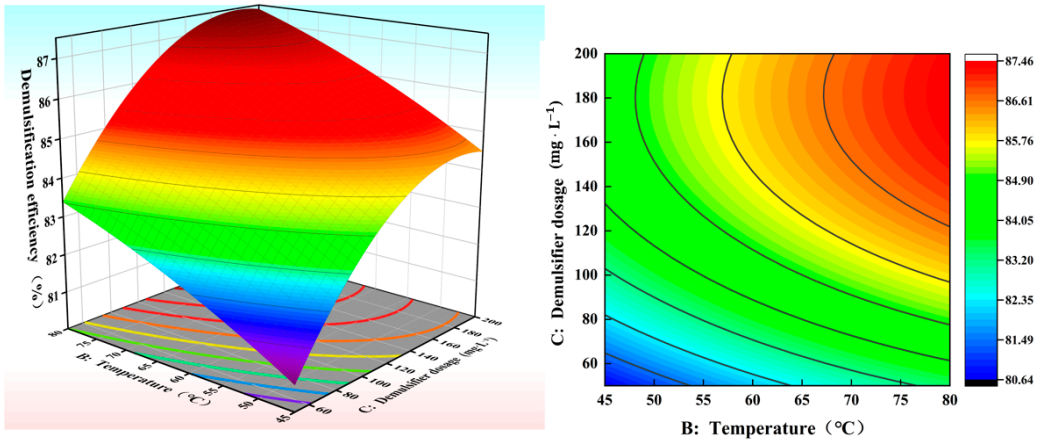

Figure 9. Three-dimensional response surface and contour plots of the RSM results: interaction effects between B and C.

Single-objective response surface optimization was conducted to maximize demulsification efficiency, using efficiency as the only response and imposing no other constraints. The model predicted optimal conditions of 7016 r/min (RCF = 6328.76 g), a system temperature of 74.8 °C, and a demulsifier dosage of 172.3 mg·L^{-1}, with an overall desirability of 1.00 and a predicted demulsification efficiency of 88.97%, as shown in Figure 10. Each predicted optimal factor value fell within the Box–Behnken design range (6000–8000 r/min, 60–80 °C, and 100–200 mg·L^{-1} demulsifier concentration). This was interpolation within the design space rather than extrapolation beyond it. The predicted efficiency was slightly above the highest measured efficiency in the experimental matrix, a normal outcome when finding the extremum of a fitted quadratic regression surface. Subsequent parallel validation experiments showed that the model's adequate precision was 97.88, far above the critical value of 4, indicating an adequate signal-to-noise ratio and practical reference value for these predicted conditions.

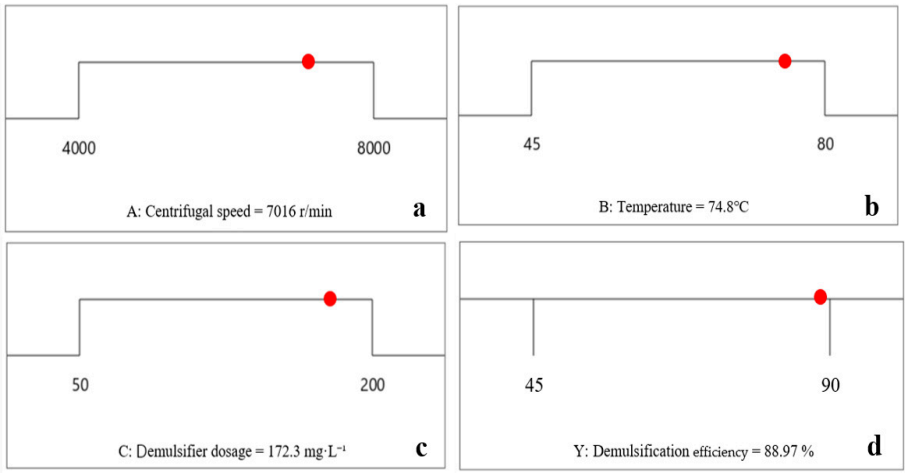

Figure 10. Optimization plot of experimental conditions. (**a**) Response optimization for centrifugal speed; (**b**) Response optimization for temperature; (**c**) Response optimization for demulsifier dosage; (**d**) Predicted demulsification efficiency at the optimized parameter combination.

3.4.3. Effect of Centrifugation Additive Content on Demulsification Performance

The effect of centrifugal additive dosage on demulsification of highly emulsified Shixi crude oil was examined at a demulsifier concentration of 50 mg·L^{-1}, centrifugal speed of 6000 r/min (RCF = 4628.52 g), system temperature of 45 °C, and centrifugation time of 10 min (under the response surface optimum, baseline demulsification was already high, and the change caused by additive dosing was limited and easily obscured by experimental error, making additive effects difficult to identify clearly. Moderately effective baseline conditions were therefore selected for single-factor experiments. The optimal process conditions from the response surface design would subsequently be combined with the optimal additive dosages identified during screening for parallel validation). The results are shown in Figure 11.

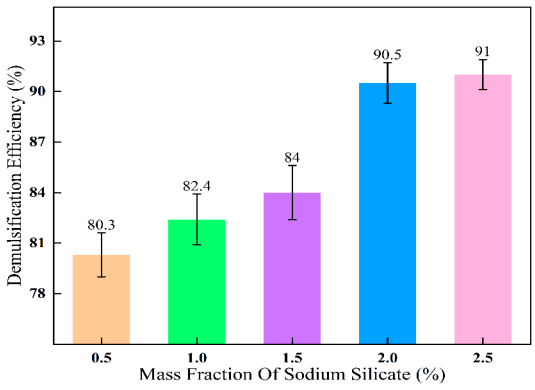

Figure 11. Effect of sodium silicate dosage on the demulsification efficiency of highly emulsified crude oil.

Sodium silicate increased demulsification efficiency. By analogy with the experimental observations and existing literature, the proposed mechanism is that sodium silicate may form silica sol between solid particles in oily sludge and establish a porous framework, maintaining high permeability and creating interconnected channels that promote release of water trapped in the sludge, thereby improving demulsification. This hypothesis will be further tested in subsequent characterization experiments. As sodium silicate dosage increased from 0.5 wt% to 2.5 wt%, demulsification efficiency generally rose. At dosages of 0.5%, 1.0%, and 1.5%, efficiencies were 80.3%, 82.4%, and 84.0%, respectively, a relatively

small increase. Raising the dosage from 1.5% to 2.0% markedly increased efficiency to 90.5%, an increase of 6.5 percentage points, indicating that a suitable amount of sodium silicate substantially promoted oil–water separation. Increasing dosage further to 2.5% raised efficiency only to 91.0%, 0.5 percentage points above that at 2.0%, indicating a markedly diminished gain and gradual saturation of the promoting effect beyond 2.0%.

Considering the increase in demulsification efficiency, chemical consumption, and field treatment requirements, an appropriate sodium silicate dosage of 2.0% was selected. At this dosage, efficiency reached 90.5% and good oil–water separation was achieved. Raising the dosage to 2.5% produced little additional improvement. Thus, 2.0% can be recommended for subsequent optimization and performance evaluation of the centrifugal demulsification process.

Under the same baseline experimental conditions, the effect of flocculant SP169 dosage on centrifugal demulsification was also examined, as shown in Figure 12.

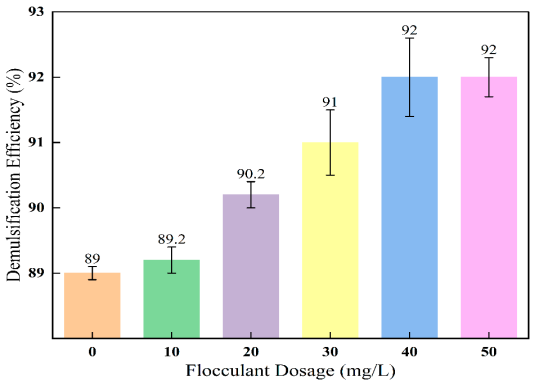

Figure 12. Effect of flocculant (SP169) on demulsification.

SP169 can adsorb at the oil–water interface, displace the natural resin–asphaltene interfacial film, and promote coalescence of free water droplets. As the mass concentration of SP169 increased, demulsification efficiency generally rose. Increasing SP169 dosage from 0 to 20 mg·L^{-1} gradually raised efficiency from 89.0% to 90.2%, indicating that an appropriate SP169 dose could promote emulsion demulsification and separation. At 30 and 40 mg·L^{-1}, efficiency increased to 91.0% and 92.0%, respectively. Based on the experimental observations and existing literature, the proposed mechanism is that SP169 may weaken the stabilizing effect of particles at the oil–water interface through interfacial-film displacement and adsorption bridging [37], promoting droplet collision, coalescence, and settling. This hypothesis will be further tested in subsequent characterization experiments.

When SP169 dosage was raised further to 50 mg·L^{-1}, efficiency remained 92.0%, essentially the same as at 40 mg·L^{-1}, indicating that additional flocculant did not appreciably improve demulsification. This may be because the suspended particles and dispersed water droplets available for removal by flocculation had largely aggregated and separated; excessive flocculant could not further improve efficiency and might instead increase chemical consumption and downstream treatment burden.

Therefore, under these experimental conditions, efficiency reached its maximum of 92.0% at 40 mg·L^{-1} SP169, and higher dosage produced no evident additional benefit. Considering demulsification performance and chemical economics, an appropriate SP169 dosage of approximately 40 mg·L^{-1} is recommended.

3.4.4. Effect of Centrifugation Time on Demulsification Performance

To identify the independent effect of centrifugation time more clearly, a single-factor experiment was performed under moderately effective baseline conditions. Demulsifier

concentration was fixed at 50 mg·L^{-1}, centrifugal speed at 6000 r/min (RCF = 4628.52 g), system temperature at 45 °C, sodium silicate mass fraction at 2.0%, and flocculant SP169 dosage at 20 mg·L^{-1}; only centrifugation time was changed. Figure 13 shows its effect on demulsification efficiency. Within the range studied, efficiency generally increased with time. From 1 to 3 min, efficiency rose from approximately 53% to 68%, an increase of approximately 15 percentage points, and reached approximately 73% at 5 min. At 8 min, efficiency increased rapidly to approximately 88%, indicating that an appropriate increase in centrifugation time promoted droplet migration and coalescence and oil–water phase separation. From 8 to 10 min, efficiency rose only from approximately 88% to 92%, a markedly smaller increase, suggesting that demulsification gradually approached equilibrium and further extension provided limited improvement.

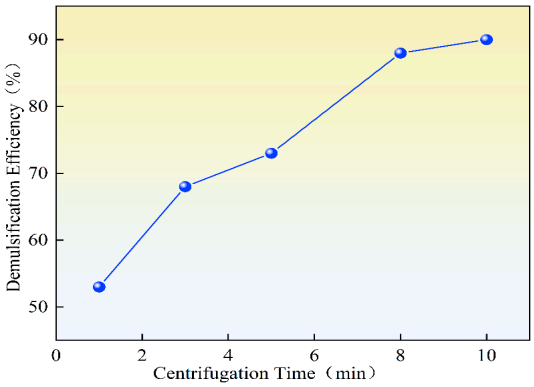

Figure 13. Effect of centrifugation time on demulsification efficiency.

Overall, a relatively high demulsification efficiency of approximately 88% was obtained after 8 min of centrifugation, differing by only about 2 percentage points from that at 10 min. Therefore, when both demulsification and treatment efficiency are considered, 8 min may be preferentially used as an appropriate centrifugation time in subsequent experiments. If the main objective is to obtain the highest demulsification efficiency, time can be extended to 10 min.

3.4.5. Validation of Combined Response Surface Conditions and Additives

The Box–Behnken response surface model optimized only three core process variables: centrifugal speed, system temperature, and demulsifier concentration. Sodium silicate and SP169 were not included in the statistical design. Single-factor screening of additives was conducted under moderately effective baseline conditions to distinguish the effects of the two additives independently. This section reports confirmatory validation experiments, not multivariable joint optimization: the main process parameters obtained from response surface optimization were combined with the appropriate additive dosages identified by earlier single-factor screening. The experimental conditions were a centrifugal speed of 7016 r/min (RCF = 6299.93 g), system temperature of 74.8 °C, demulsifier dosage of 172.3 mg·L^{-1}, sodium silicate mass fraction of 2.0%, SP169 dosage of 40 mg·L^{-1}, and centrifugation time of 10 min. Three independent parallel experiments were conducted. All other procedures and sample conditions were the same as in the preceding experiments. The results are presented in Table 2.

Table 2. Parallel validation of demulsification efficiency under optimal process conditions and the oil–water–solid material balance.

Experiment No.	Centrifugal Speed/r·min^{-1}	Demulsifier Concentration/ mg·L^{-1}	Temperature/°C	Sodium Silicate Mass Fraction/%	SP169/ mg·L^{-1}	Centrifugation Time/min	Volumetric Demulsification Efficiency η_v/%	Residual Water Content of Oil Phase/%	Mass-Based Demulsification Efficiency η_M/%	Water Retained in Solid Phase/Total Water, %
1	7016	172.3	74.8	2.0	40	10	93.2	3.12	89.7	3.8
2	7016	172.3	74.8	2.0	40	10	93.8	2.87	90.4	3.6
3	7016	172.3	74.8	2.0	40	10	93.5	2.99	90.1	3.7
Mean	7016	172.3	74.8	2.0	40	10	93.5 ± 0.30	2.99 ± 0.13	90.1 ± 0.35	3.7 ± 0.11

The demulsification efficiencies in the three parallel experiments were 93.2%, 93.8%, and 93.5%, respectively. The mean efficiency calculated from the volume of separated free water was 93.5 ± 0.30%. Overall, the validation results showed that combining the process parameters from response surface optimization with the appropriate additives could achieve higher demulsification efficiency, confirming the good oil–water separation performance of the centrifugation process combined with additives for highly emulsified Shixi crude oil with a high solids content.

The material balance in Table 2 shows that some water in the high-solids system was trapped by solid–organic matter agglomerates. Consequently, the demulsification efficiency calculated by the volumetric method was slightly higher than the mass-based efficiency based on residual oil-phase water content measured with the JSH3202 analyzer. Under the optimal conditions, however, water trapped in the solid phase accounted for only approximately 3.7% of total water, and the two methods yielded similar results, indicating that the aqueous phase was released relatively completely and that the volumetric result was useful for reference.

3.4.6. Microscopic Observations Before and After Centrifugation of Highly Emulsified Crude Oil

To qualitatively analyze the effects of centrifugation on dispersion and phase separation in highly emulsified crude oil, optical microscopic observations were made before and after centrifugal demulsification. The results are shown in Figure 14.

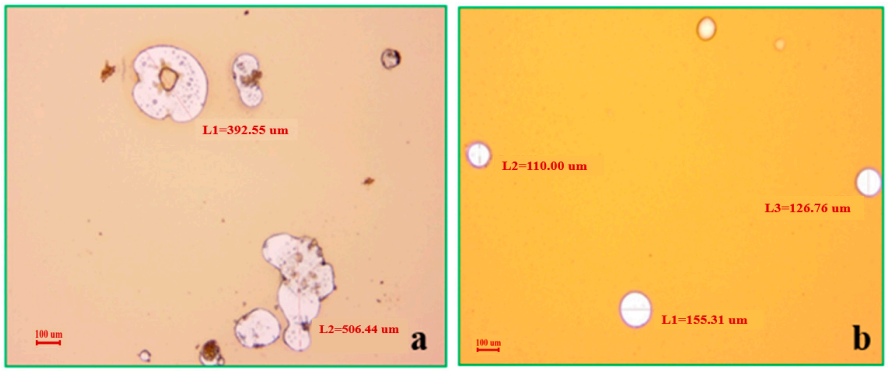

Figure 14. Microscopic morphology of the highly emulsified crude oil emulsion system before and after centrifugal demulsification: (**a**) aggregate structures in the emulsion layer before demulsification; (**b**) sample morphology after centrifugal demulsification.

Before centrifugation, the sample was observed microscopically without adding demulsifier or other reagents and without heating. As shown in Figure 14a, conspicuous irregular aggregates could be observed in the emulsified crude oil. The annotated dimensions of 392.55 μm and 506.44 μm are examples of typical aggregates in this field of view and do

not represent the overall statistical mean particle size of the sample. These aggregates comprised multiple dispersed droplets, oil–water interfacial-film components, and solid particles, reflecting the formation of loose, irregularly bounded aggregates of fine water droplets through the combined action of resins, asphaltenes, and inorganic solid particles.

The presence of these aggregates indicates that, although dispersed water droplets had aggregated to some extent, their interfaces remained stabilized by the particle-containing composite interfacial film. The droplets therefore could not readily coalesce further, and rapid oil–water stratification under static conditions was difficult. The small oil–water density difference further reduced the driving force for droplet migration and separation, maintaining the high stability of the emulsion.

After treatment under the combined optimal response surface and additive conditions, the microscopic morphology and overall dispersion state changed markedly, as shown in Figure 14b. In these fields of view, the proportion of large, irregular aggregates decreased, and apparent system uniformity increased, indicating that the strong centrifugal force field promoted relative migration among droplets, oil, water, and suspended particles. During centrifugation, fine droplets were more likely to migrate directionally, collide, and coalesce under strong centrifugal forces. At the same time, the combined effects of sodium silicate and flocculant could weaken the stabilizing action of solid particles at the oil–water interface, promoting disruption of the interfacial film and droplet coalescence. As droplet size increased, the driving force for separation of the oil and water phases increased further, ultimately achieving effective separation of oil, water, and solid particles.

3.5. Economic Analysis

To compare the experimental results of the three demulsification processes under their respective optimal conditions, the best operating conditions and corresponding demulsification performance obtained from the single-factor experiments for each process are summarized in Table 3. The conditions in the table were optimized separately for each process. The three processes were not operated at entirely identical temperatures, treatment times, or reagent systems, so these data provide a horizontal reference for process screening rather than a rigorous quantitative comparison under identical conditions.

Table 3. Summary of the optimal experimental conditions and demulsification performance of the three processes.

Process	Temperature/°C	Treatment Time/min	Reagent System	Demulsification Efficiency (Volumetric)/%	Remarks
Electrostatic dehydration and demulsification	60	60	Demulsifier I, 200 mg·L^{-1}	52.6	Device voltage limit 5.85 kV; risk of electric-field trips
Ultrasonic demulsification	80	10	Demulsifier I, 200 mg·L^{-1}	40.0	Bath-type, non-probe ultrasonication; set power 150 W
Centrifugal demulsification combined with additives	74.8	10	Demulsifier I 172.3 mg·L^{-1} + sodium silicate 2.0% + SP169 40 mg·L^{-1}	93.5 ± 0.30	Response surface conditions combined with additives for validation

On this screening basis, the processes were further compared across engineering dimensions, including demulsification efficiency, treatment cycle, footprint, and adaptability. The results are presented in Table 4.

Table 4. Overall comparison of different demulsification processes.

Comparison Criterion	Conventional Thermochemical Settling	Electrostatic Dehydration Process	Centrifugal Demulsification Combined with Additives
Maximum demulsification efficiency	Approximately 45%	52.6%	93.5%
Treatment cycle per batch	24–48 h	1–2 h	10~30 min
Treatment cost per tonne/(CNY·t^{-1})	Approximately 85	Approximately 120	105.31
Footprint	Large (large settling tank)	Medium	Small (skid-mounted layout possible)
Adaptability to high-solids emulsions	Poor	Poor (conductive FeS facilitates electric breakdown)	Good
Level of automation	Low	Medium	High

To objectively evaluate the engineering application value of the centrifugal demulsification process combined with additives, a techno-economic calculation was conducted for an annual treatment capacity of 1×10^4 t of highly emulsified crude oil, using field operating conditions and the energy structure of the Shixi Operating Area of the Xinjiang Oilfield. The calculation boundaries were as follows: the unit operates continuously for 8000 h per year, average annual feed crude oil temperature is 20 °C, and treatment temperature is 74.8 °C; oilfield associated gas is the heating source, and industrial electricity prices, associated-gas prices, and physical-property parameters are based on actual field settlement figures. The complete skid-mounted unit includes an industrial horizontal decanter centrifuge, heat exchange, chemical dosing, storage and transportation, and automatic control systems. Total fixed-asset investment is CNY 3 million, with straight-line depreciation over 10 years and a 5% residual value. Chemical dosages use the optimal process parameters from this study, and chemical prices refer to average oilfield industrial procurement prices. Separated water and oily sludge are disposed of using the station's existing systems. The economic analysis in the original text had obvious deficiencies: it directly applied the power parameters of a laboratory benchtop centrifuge to calculations for an industrial unit and omitted heating energy consumption, some chemicals, labor and maintenance, and waste disposal costs. These have been corrected in this revision.

This study used full-cost accounting, considering all relevant expenses for unit operation, chemicals, labor, equipment depreciation, and waste disposal. The detailed costs are shown in Table 5. The calculated total annual cost was CNY 1.0531 million, corresponding to a crude oil treatment cost of CNY 105.31 per tonne.

The process benefit mainly arises from enabling emulsified crude oil to meet export specifications and avoiding resource losses caused by downgrading. According to the Shixi Operating Area's field calculation, the downgrade loss for this difficult-to-treat emulsified crude oil is approximately CNY 542 per tonne. At the process's mean demulsification efficiency of 93.5%, annual total benefit is CNY 5.42 million. After deducting total costs, annual net profit is CNY 4.3669 million, and the simple payback period is 0.69 years, indicating a favorable return on investment. A single-factor sensitivity analysis was conducted to assess the effects of changes in external conditions on project profitability, as shown in Table 6. Treatment scale and crude oil value-added benefit were moderately sensitive factors, while fluctuations in chemical and energy prices had little effect on profitability. Even if treatment

scale and benefit both decrease by 20%, annual net profit remains above CNY 3 million, indicating strong resilience to risk.

Table 5. Economic benefit assessment of the centrifugal demulsification process combined with additives.

Item	Calculation Basis	Calculation Rate	Annual Cost/CNY 10,000	Remarks
Electricity cost	Annual electricity use 200,000 kW·h	CNY 0.44/ (kW·h)	8.80	Centrifuge + pumps and valves + automatic control system
Heating gas cost	Annual gas use 50,800 m^3	CNY 0.80/m^3	4.06	Associated-gas heating to 74.8 °C
Demulsifier cost	Annual use 1.75 t	CNY 8650/t	1.51	Dosage 172.3 mg/L
Sodium silicate cost	Annual use 200 t	CNY 800/t	16.00	Dosage 2.0% (mass fraction)
SP169 flocculant cost	Annual use 0.4 t	CNY 12,000/t	0.48	Dosage 40 mg/L
Labor cost	4 operators	CNY 80,000/per son·year	32.00	Continuous operation in four crews and three shifts
Equipment operation and maintenance cost	Fixed assets CNY 3 million	Annual provision 2.5%	7.50	Maintenance + replacement of wear parts
Waste disposal cost	Wastewater 3325 t + sludge 150 t	-	2.80	Wastewater sent to the station system + compliant sludge disposal
Equipment depreciation	Fixed assets CNY 3 million	Straight-line depreciation over 10 years	28.50	Residual value 5%
Other management and laboratory costs	Direct operating cost	Provision 5%	3.66	Management, laboratory testing, and miscellaneous consumables
Total annual cost	-	-	105.31	Full cost
Crude oil treatment cost per tonne	Annual treatment 1×10^4 t	-	CNY 105.31/t	Equivalent to CNY 0.0105 × 10,000/t

Table 6. Results of economic sensitivity analysis.

Variable	Change	Annual Net Profit/CNY 10,000	Change in Net Profit	Sensitivity
Baseline	0	436.69	-	-
Treatment scale	+20%	545.09	+24.82%	Moderately sensitive
Treatment scale	−20%	328.29	−24.82%	Moderately sensitive
Crude oil value-added benefit	+20%	545.09	+24.82%	Moderately sensitive
Crude oil value-added benefit	−20%	328.29	−24.82%	Moderately sensitive
Chemical price	+20%	433.09	−0.82%	Low sensitivity
Chemical price	−20%	440.29	+0.82%	Low sensitivity
Energy price	+20%	434.13	−0.59%	Low sensitivity
Energy price	−20%	439.25	+0.59%	Low sensitivity

4. Conclusions

This study investigated a high-solids W/O crude oil emulsion from a settling tank in the Shixi Operating Area of the Xinjiang Oilfield. After analyzing its basic properties, solid-phase composition, and stability characteristics, the treatment adaptability of electrostatic dehydration, ultrasonic demulsification, and centrifugal demulsification was compared. Single-factor experiments and Box–Behnken response surface methodology were then used to optimize the centrifugal demulsification process combined with additives. The main conclusions are as follows:

The emulsion had an initial water content of 35.56% and a suspended-solids content as high as 8300 mg/L. The solid phase consisted mainly of FeS, $CaCO_3$, and SiO_2. Resins, asphaltenes, and inorganic solid particles jointly formed a stable composite interface, while

the relatively small oil–water density difference further made demulsification difficult and limited the effectiveness of conventional treatment processes.

Process screening showed that, under their respective optimized operating conditions, electrostatic dehydration achieved a maximum demulsification efficiency of 52.6% but was subject to electric-field instability and tripping risk because of the high content of conductive FeS particles. Ultrasonic demulsification reached a maximum of only 40.0%, with an apparent attenuation of cavitation by solid particles. Neither process met the high-efficiency treatment needs of this system. Centrifugal demulsification showed stronger separation capability for this high-solids system. After optimizing the main process parameters by response surface methodology and combining sodium silicate and SP169 additives, the volumetric demulsification efficiency reached 93.5 ± 0.30% under optimal conditions.

This study was based on laboratory batch experiments using a single batch of field samples. Continuous-flow and pilot-scale scale-up experiments have not yet been conducted. Scale-up effects relevant to engineering application, including treatment throughput, solid-phase accumulation and discharge, equipment scaling, and long-term operational stability, require further investigation using multiple sample batches and pilot-scale tests. These results provide a reference for selecting demulsification processes and optimizing laboratory process parameters for high-solids crude oil emulsions in Shixi and under similar operating conditions.

Author Contributions: Conceptualization, J.H. and L.L.; methodology, L.L., B.L., X.P. and J.H.; validation, L.L., B.L., X.P., Y.L. and J.W.; formal analysis, L.L., B.L. and X.P.; investigation, L.L., B.L., X.P., Y.L., J.W. and X.Y.; resources, J.H. and X.Y.; data curation, L.L.; writing—original draft preparation, L.L.; writing—review and editing, L.L., B.L., X.P. and J.H.; visualization, L.L.; supervision, J.H.; project administration, J.H.; funding acquisition, J.H. All authors have read and agreed to the published version of the manuscript.

Funding: This work was financially supported by the Xinjiang Uygur Region "One Case, One Policy" Strategic Talent Introduction Project (No. XQZX20240054), the Innovative Talents specific project Foundation of Karamay (No. XQZX20240089), and the "Tianshan Talents" Foundation (2023TSYCJC0065) of Xinjiang Uygur Autonomous Region and the National Natural Science Foundation of China (52360003).

Data Availability Statement: The original contributions presented in this study are included in the article. Further inquiries can be directed to the corresponding authors.

Acknowledgments: The authors thank the State Key Laboratory of Heavy Oil Processing for providing the experimental platform and technical support for this work.

Conflicts of Interest: Author Xianglu Yang was employed by the company Shunan Gas Mine, PetroChina Southwest Oil and Gasfield Company. The remaining authors declare that the research was conducted in the absence of any commercial or financial relationships that could be construed as a potential conflict of interest.

Appendix A

Table A1. Response Surface Experimental Design.

Item	A: Centrifugal Speed/r/min	B: Temperature/°C	C: Demulsifier Dosage/mg·L^{-1}	Y: Demulsification Efficiency/%
1	4000	45	100	49.2
2	4000	60	200	52.6
3	4000	60	50	47.5
4	4000	80	100	51.3
5	8000	45	100	84.1

Table A1. *Cont.*

Item	A: Centrifugal Speed/r/min	B: Temperature/°C	C: Demulsifier Dosage/mg·L^{-1}	Y: Demulsification Efficiency/%
6	8000	60	50	83.2
7	8000	60	200	87.6
8	8000	80	100	88.3
9	6000	45	50	81.4
10	6000	80	50	83.7
11	6000	45	200	84.2
12	6000	80	200	87.1
13	6000	60	100	84.6
14	6000	60	100	84.2
15	6000	60	100	85
16	6000	60	100	84.5
17	6000	60	100	84.8

Table A2. Significance analysis of RSM test results.

Item	SS	df	MS	F	*p*	Significance
Model	3732.70	9	414.74	1440.84	<0.0001	significant
A	2390.62	1	2390.62	8305.10	<0.0001	
B	15.87	1	15.87	55.12	0.0001	
C	30.61	1	30.61	106.35	<0.0001	
AB	1.16	1	1.16	4.03	0.0846	
AC	0.1706	1	0.1706	0.59	0.4666	
BC	0.0077	1	0.0077	0.0267	0.8749	
A^2	1129.62	1	1129.62	3924.34	<0.0001	
B^2	0.1932	1	0.1932	0.6712	0.4396	
C^2	5.39	1	5.39	18.73	0.0034	
Residual	2.01	7	0.2878	-	–	
Lack of fit	1.65	3	0.5490	5.97	0.0583	not significant
Pure error	0.3680	4	0.0920	–	–	–
	$R^2 = 0.9995$				$R^2_{adj} = 0.9988$	
Adequate-precision	97.8814	–	–	–	–	–

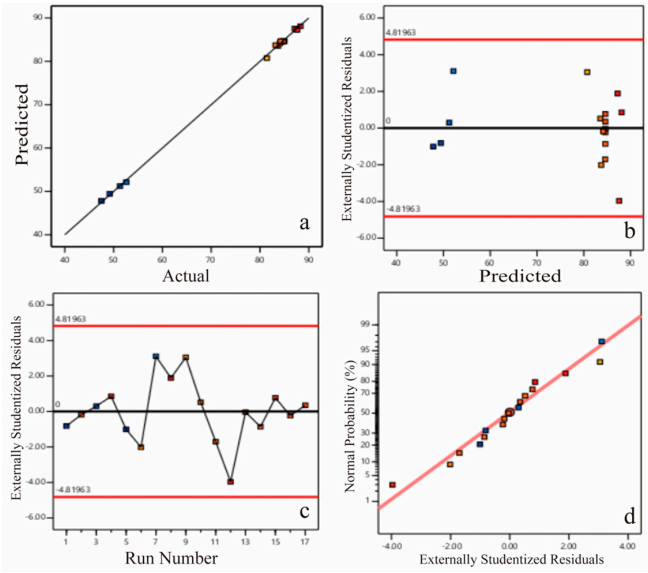

Figure A1. Residual diagnostic plots for the response surface model: (**a**) predicted versus measured values; (**b**) residuals versus predicted values; (**c**) residuals versus run number; (**d**) normal probability plot of residuals.

References

1. Yang, X.; Chen, S.; Chen, H.; He, L.; Ni, Y.; Liu, S.; Chen, Z.; Tian, Y. Comprehensive review of stabilising factors, demulsification methods, and chemical demulsifiers of oil-water emulsions. *Sep. Purif. Technol.* **2025**, *358*, 130206. [CrossRef]
2. Yonguep, E.; Kapiamba, K.F.; Kabamba, K.J.; Chowdhury, M. Formation, stabilization and chemical demulsification of crude oil-in-water emulsions: A review. *Pet. Res.* **2022**, *7*, 459–472. [CrossRef]
3. Faizullayev, S.; Adilbekova, A.; Kujawski, W.; Mirzaeian, M. Recent demulsification methods of crude oil emulsions—Brief review. *J. Pet. Sci. Eng.* **2022**, *215*, 110643. [CrossRef]
4. Low, J.Y.; Khe, C.S.; Usman, F.; Hassan, Y.M.; Lai, C.W.; You, K.Y.; Lim, J.W.; Khoo, K.S. Review on demulsification techniques for oil/water emulsion: Comparison of recyclable and irretrievable approaches. *Environ. Res.* **2024**, *243*, 117840. [CrossRef] [PubMed]
5. Liu, J.-X.; Zhu, H.-J.; Wang, P.; Pan, J.-M. Recent studies of Pickering emulsion system in petroleum treatment: The role of particles. *Pet. Sci.* **2021**, *18*, 1551–1563. [CrossRef]
6. Hernandez-Rodriguez, G.; Tenorio-Garcia, E.; Ettelaie, R.; Lishchuk, S.V.; Harbottle, D.; Murray, B.S.; Sarkar, A. Demulsification of Pickering emulsions: Advances in understanding mechanisms to applications. *Soft Matter* **2024**, *20*, 7344–7356. [CrossRef] [PubMed]
7. Sun, X.; Zeng, H.; Tang, T. Molecular Simulations on the Coalescence of Water-in-Oil Emulsion Droplets with Non-ionic Surfactant and Model Asphaltene. *Langmuir* **2023**, *39*, 2233–2245. [CrossRef] [PubMed]
8. Song, S.; Li, C.; Jia, W.; Maeda, N.; Zhang, X.; Xiao, H.; Yang, F.; Zhang, Y. Adsorption behavior of non-ionic demulsifiers at the oil/water interface stabilized by asphaltenes: Experiments, adsorption kinetics, and mechanisms. *Sep. Purif. Technol.* **2025**, *355*, 129703. [CrossRef]
9. Ma, H.; Yang, D.; Li, Z.; Sun, Y.; Hu, Y.; Mao, X.; Lu, B.; Zhang, H.; Zeng, H. Probing the adsorption behavior and molecular interactions of asphaltene subfractions at Water–Toluene/Heptol interface. *Fuel* **2025**, *389*, 134577. [CrossRef]
10. Song, F.; Zheng, H.; Li, T.; Fu, X.; Feng, C.; Ma, C.; Jiang, S.; Wang, J.; Huang, Y.; Zhou, F. The influence of asphaltene and resin on the stability of crude oil emulsion and its demulsification mechanism. *J. Mol. Liq.* **2024**, *413*, 125924. [CrossRef]
11. Lu, R.; Lai, L.; Zhang, H. Stabilization mechanism of emulsion gels of crude oil with low asphaltene, resin, and wax contents. *J. Mol. Liq.* **2025**, *417*, 126496. [CrossRef]
12. Sun, G.-Y.; Zhang, H.; Liu, D.-W.; Li, C.-X.; Yang, F.; Yao, B.; Duan, Z.; Chen, X.-Y.; Sheng, F.-J. Co-adsorption behavior of aggregated asphaltenes and silica nanoparticles at oil/water interface and its effect on emulsion stability. *Pet. Sci.* **2022**, *19*, 1793–1802. [CrossRef]
13. Hattori, T.; Elakneswaran, Y.; Hao, X.; Shimokawara, M.; Hiroyoshi, N. Influence of inorganic solid particles on the stability of water-in-crude oil emulsions: Evaluating the role of surface charge. *Colloids Surf. A Physicochem. Eng. Asp.* **2024**, *699*, 134726. [CrossRef]
14. Zhang, X.; He, C.; He, L.; Sui, H.; Li, X. Breaking oil–water emulsions co-stabilized by $CaCO_3$ solids and natural stabilizers: Efficient strategy and mechanisms. *Chem. Eng. Sci.* **2026**, *320*, 122627. [CrossRef]
15. Hristova, E.; Stoyanov, S.R.; McFarlane, R.; Nikooyeh, K. Investigation of Unresolved Interface "Rag Layer" in Athabasca Oil Sand Bitumen In Situ Recovery. *ACS Omega* **2024**, *9*, 32201–32209. [CrossRef] [PubMed]
16. Freitas, I.G.; Perles, C.E.; Guersoni, V.C.B.; Pessanha, T.M.; Bannwart, A.C. Interfacial Tension as a Parameter to Assess Demulsifier Efficiency on Heavy Crude Oil Emulsions. *ACS Omega* **2025**, *10*, 34142–34150. [CrossRef] [PubMed]
17. Shen, L.; Ai, G.; Liu, H.; Zhu, L.; Lai, L.; Yan, X.; Yu, W.; Mi, Y. Synthesis and demulsification performance of a novel low-temperature demulsifier based on trimethyl citrate. *J. Hazard. Mater.* **2024**, *472*, 134543. [CrossRef] [PubMed]
18. Zhao, Y.; Huang, M.; Wang, X.; Ding, Y.; Chen, L.; Qu, Q.; Tang, Y.; Mi, Y. A simple two-step reaction for synthesizing demulsifiers for a high salt crude oil emulsion. *Sep. Purif. Technol.* **2025**, *359*, 130494. [CrossRef]
19. Husain, A.; Adewunmi, A.A.; Gbadamosi, A.; Al-Harthi, M.A.; Patil, S.; Kamal, M.S. Demulsification of asphaltene stabilized crude oil emulsions by biodegradable ethylcellulose polymers with varying viscosities. *Sci. Rep.* **2023**, *13*, 1090. [CrossRef] [PubMed]
20. Velayati, A.; Habibi, A.; Nikrityuk, P.; Tang, T.; Zeng, H. Emulsions in Bitumen Froth Treatment and Methods for Demulsification and Fines Removal in Naphthenic Froth Treatment: Review and Perspectives. *Energy Fuels* **2022**, *36*, 8607–8623. [CrossRef]
21. Farooq, U.; Patil, A.; Panjwani, B.; Simonsen, G. Review on Application of Nanotechnology for Asphaltene Adsorption, Crude Oil Demulsification, and Produced Water Treatment. *Energy Fuels* **2021**, *35*, 19191–19210. [CrossRef]
22. Sjöblom, J.; Mhatre, S.; Simon, S.; Skartlien, R.; Sørland, G. Emulsions in external electric fields. *Adv. Colloid Interface Sci.* **2021**, *294*, 102455. [CrossRef] [PubMed]
23. Kou, J.; Huang, K.; Li, Z. Study on demulsification characteristics of crude oil based on orthogonal dual frequency ultrasonic standing wave field. *Colloids Surf. A Physicochem. Eng. Asp.* **2024**, *695*, 134280. [CrossRef]
24. Wang, Y.; Du, C.; Yan, Z.; Duan, W.; Deng, J.; Luo, G. Rapid demulsification and phase separation in a miniaturized centrifugal demulsification device. *Chem. Eng. J.* **2022**, *446*, 137276. [CrossRef]

25. *SY/T 5281-2000*; Bottle Test Method for the Demulsification Performance of Crude Oil Demulsifiers. Petroleum Industry Press: Beijing, China, 2000.
26. *SY/T 5329-2012*; Water Quality Standard and Practice for Analysis of Oilfield Injecting Waters in Clastic Reservoirs. Petroleum Industry Press: Beijing, China, 2012.
27. Kooti, G.; Dabir, B.; Taherdangkoo, R.; Butscher, C. Modelling droplet size distribution in inline electrostatic coalescers for improved crude oil processing. *Sci. Rep.* **2023**, *13*, 20209. [CrossRef] [PubMed]
28. Hasib, R.; Anand, V.; Naik, V.M.; Juvekar, V.A.; Thaokar, R.M. Mitigating Noncoalescence and Chain Formation in an Electrocoalescer by Electric Field Modulation. *Ind. Eng. Chem. Res.* **2022**, *61*, 17145–17155. [CrossRef]
29. Li, N.; Sun, Z.; Sun, J.; Liu, W.; Wei, L.; Li, T.; Li, B.; Wang, Z. Deformation and breakup mechanism of water droplet in acidic crude oil emulsion under uniform electric field: A molecular dynamics study. *Colloids Surf. A Physicochem. Eng. Asp.* **2022**, *632*, 127746. [CrossRef]
30. Akram, W.; Zhang, X.; Wang, Z.; Muhmmad Mostafa, M.Y.; Gunawardane, A.; Yang, Z.; He, L.; Sui, H. Understanding the demulsification of highly waxy shale oil emulsions by oxygen-rich demulsifiers. *Fuel* **2025**, *401*, 135766. [CrossRef]
31. Adewunmi, A.A.; Hussain, S.M.S.; Patil, S.; Kamal, M.S. Influence of Varying Oil–Water Contents on the Formation of Crude Oil Emulsion and Its Demulsification by a Lab-Grown Nonionic Demulsifier. *ACS Omega* **2024**, *9*, 19620–19626. [CrossRef] [PubMed]
32. Romanova, Y.N.; Koroleva, M.Y.; Musina, N.S.; Maryutina, T. Ultrasonic demulsification of water-in-crude oil emulsions: Influence of rheological properties. *Chem. Eng. Process. Process Intensif.* **2025**, *211*, 110242. [CrossRef]
33. Adeyemi, I.; Meribout, M.; Khezzar, L.; Kharoua, N.; AlHammadi, K. Techno-economic comparative assessment of the ultrasound, electrostatic and microwave supported coalescence of binary water droplets in crude oil. *Ultrason. Sonochem.* **2023**, *95*, 106402. [CrossRef] [PubMed]
34. Lü, Y.; Zhu, S.; Lin, G.; Wang, M.; Wang, C. Research on ultrasonic demulsification characteristics and parameter optimization of condensate oil emulsion. *Chem. Eng. Process. Process Intensif.* **2025**, *209*, 110185. [CrossRef]
35. Tahami, S.; Movagharnejad, K. Demulsification of water in crude oil emulsions via phosphonium-based ionic liquids: Statistical modeling and optimization. *J. Mol. Liq.* **2024**, *411*, 125748. [CrossRef]
36. Ahmadi, S.; Khormali, A.; Meerovich Khoutoriansky, F. Optimization of the demulsification of water-in-heavy crude oil emulsions using response surface methodology. *Fuel* **2022**, *323*, 124270. [CrossRef]
37. Huang, Y.; Qiao, C.; Li, Z.; Zeng, H. Mechanistic insights into the role of branched polyethylenimine in breaking Asphaltene-Stabilized Oil-in-Water emulsions: Temperature effects. *Sep. Purif. Technol.* **2025**, *362*, 131913. [CrossRef]

Disclaimer/Publisher's Note: The statements, opinions and data contained in all publications are solely those of the individual author(s) and contributor(s) and not of MDPI and/or the editor(s). MDPI and/or the editor(s) disclaim responsibility for any injury to people or property resulting from any ideas, methods, instructions or products referred to in the content.